The key surface species and oxygen vacancies in $MnO_x(0.4)$-CeO_2 toward repeated soot oxidation

Hui He[a], Xueting Lin[a], Shujun Li[a], Zeng Wu[a], Jingheng Gao[a], Junliang Wu[a], William Wen[c], Daiqi Ye[a,b], Mingli Fu[a,b,*]

[a] Guangdong Provincial Key Laboratory of Atmospheric Environment and Pollution Control, School of Environment and Energy, South China University of Technology, Guangzhou, 510006, China
[b] Guangdong Provincial Engineering and Technology Research Center for Environmental Risk Prevention and Emergency Disposal, South China University of Technology, Guangzhou, 510006, China
[c] Centre for Clean Environment and Energy, Environmental Futures Centre, School of Environment, Griffith University, Gold Coast, QLD4222, Australia

ARTICLE INFO

ABSTRACT

Surface species and oxygen vacancies were studied in $MnO_x(0.4)$-CeO_2 toward repeated soot oxidation. $MnO_x(0.4)$-CeO_2 catalysts prepared by the citric acid complex method were repeatedly used in a 10% O_2/Ar gas flow and showed favorable activity and satisfactory durability toward soot oxidation. X-ray diffraction (XRD), N_2 adsorption/desorption, Electron paramagnetic resonance (EPR), X-ray photoelectron spectroscopy (XPS) and in situ visible/UV Raman characterization methods were utilized to investigate the structural features of fresh and reused catalysts. The irreversible conversion of high valence manganese species as well as the reduction of Frenkel-type oxygen vacancies and lattice oxygen could be clearly observed in the reused samples, which were associated with the slight deactivation. Spectators and participators were two existing forms of Frenkel-type oxygen vacancies. It was noteworthy that the participators almost fully regenerated after each reaction cycle, which ensured the ability to activate O_{latt} in repeated soot oxidation process. Therefore, the catalysts maintained favorable activity and satisfactory durability, which was mainly because the relatively stable level of participators.

1. Introduction

Nowadays, diesel engines predominate in the commercial vehicles due to the high fuel efficiency, reliability and durability [1,2]. However, the emission particulate matter, which is to blame for the health and environmental issues [3–5], is one of the most serious drawbacks of diesel engines. Catalytic combustion is an efficient method to remove soot particulates, exhausted from diesel engines. And the key to catalytic combustion is to develop efficient and long-life catalysts [6,7]. Currently, CeO_2 has attracted extensive attention for using in soot catalytic oxidation due to its remarkable oxygen storage capacity and facile exchange Ce^{3+}/Ce^{4+} redox couple which ensure the formation of oxygen species and oxygen vacancies [8–12]. It is believed that oxygen species and oxygen vacancies are well associated with the oxygen diffusion, exerting important influences on the catalytic activity of ceria-based catalysts [13–17].

The introduction of transition metal oxides into CeO_2 can enhance the catalytic activity of ceria-based oxides for soot oxidation because

the transition metal oxides exhibit good redox ability and can act as active components for soot oxidation [11,18–23]. In particular, Mn doped ceria catalysts show superior activity compared to ceria-based catalysts modified by other transition metals owing to the multiple chemical valence and excellent redox ability [24–27]. Compared with pure ceria, the incorporation of Mn into ceria-based catalysts can increase the concentration of oxygen vacancies, generate plenty of surface active oxygen species and improve their mobility, which significantly enhance the catalytic activities [28–32]. Evidently, the variation of structure and surface property of the MnO_x-CeO_2 mixed oxides due to the synergetic effect between MnO_x and CeO_2 would be critical for soot catalytic oxidation [29,33,34].

However, a large number of researches have focused on the catalytic property of fresh ceria-based catalysts, ignoring the depression of catalytic efficiency when they are reused, which reduction restricts their practical application [35]. It is important to study this depressed phenomenon and expound the mechanism, thus to provide relevant information on the relationship between the surface oxygen species as

well as oxygen vacancies and the activity degeneration.

Herein, we investigate the repeated soot oxidation over $MnO_x(0.4)$-CeO_2 prepared by the citric acid complex method. Especially, in situ Raman spectroscopy is employed to study the defect structure changes in $MnO_x(0.4)$-CeO_2 catalysts during the repeated soot oxidation. And XPS is used to detect the variation of the oxidation states of Mn and surface oxygen species in $MnO_x(0.4)$-CeO_2. EPR technique is utilized to identify the oxidation states of manganese species in fresh and reused $MnO_x(0.4)$-CeO_2 catalysts. The purpose of this work is to discuss the relationship between surface active species, oxygen vacancies and catalytic activity degrading in the repeated soot oxidation.

2. Experimental

2.1. Catalysts preparation

The $MnO_x(0.4)$-CeO_2 catalysts were synthetized by the citric acid complex method described in detail elsewhere [36,37]. Ce $(CH_3COO)_3·5H_2O$ and $Mn(CH_3COO)_2·4H_2O$ were employed as metal precursors, and all the reagents used were of analytical grade. 3.256 g of $Ce(CH_3COO)_3·5H_2O$ (Aladdin) and 0.49 g of $Mn(CH_3COO)_2·4H_2O$ (Aladdin) were dissolved in 20 ml of distilled water to obtain a mixed solution. Meanwhile, stoichiometric citric acid (Fuchen, Tianjin) was dissolved in distilled water, and it was added dropwise into the mixed solution under appropriate stirring condition at 70 °C in water bath until the pH value was adjusted to 1.5. Subsequently, the mixed solution was evaporated at 95 °C. It was immediately transferred to oil bath pan, when the mixed solution became gelatinous, and maintained at 150 °C until the gelatinous mixture became agglomerate. The resultant materials were dried at 120 °C for 2 h and calcined at 550 °C in air for 5 h to get $MnO_x(0.4)$-CeO_2 catalysts.

2.2. Catalytic activity measurement

The catalytic activity was evaluated by a temperature-programmed oxidation (TPO) reaction apparatus. Printex-U (Degussa) was used as a model soot. 30 mg of model soot and 270 mg of catalyst powder were mixed and milled carefully by an agate mortar for 2 min for "loose contact" conditions. In order to prevent reaction runaway, 300 mg of the soot-catalyst mixture was diluted with 900 mg of silica pellets. The mixture was placed in a tubular quartz reactor of 12 mm in inner diameter and fixed by silica wool. The reaction temperature was adjusted by the intelligence temperature controller from RT to 700 °C at a heating rate of 3 °C min^{-1}. The inlet gas mixture was 10% O_2 in argon with a flow rate of 100 ml min^{-1}. The outlet gas mixture was analyzed by a KC GC-900A equipped with TCD and TDX-01. The ignition temperature (T_i) and burnout temperature (T_c) represented the temperature at which the CO_2 concentration reached 5000 ppm and returned to 1000 ppm in the outlet gas, respectively. T_m represented the temperature of maximal soot oxidation rate. ΔT ($\Delta T = T_c - T_i$) represented the combustion interval.

2.3. Catalysts characterization

XRD patterns were collected on a Bruker D8 Advance powder diffractometer using a Ni β-filtered Cu Kα radiation (λ = 0.15418 nm), operating at 40 mA and 40 kV. The scanning 2θ range was 20–90° with a scan step of 0.02°.

Nitrogen adsorption and desorption isotherms were measured at 77 K using an ASAP 2020N Autosorb surface analyzer from Micromeritics. The fresh and reused samples were degassed in vacuum chamber for 4 h at 300 °C before the measurement. The specific surface area was calculated using the BET model.

EPR measurements were performed at room temperature on a Bruker EMX spectrometer operating at the X-band (9.87 GHz) frequency. The magnetic field was modulated at 100 kHz, and the power

supply was 1.85 mW. The g values were determined by the frequency and magnetic field values.

XPS signals were acquired on ESCA250 electron spectrometer from Thermo-VG with a monochromatic Mg Kα radiation (hv = 1253.6 eV) as the excitation source. Charging of samples was corrected by setting the binding energy of adventitious carbon (C 1s) at 284.6 eV.

Raman spectra were obtained with HORIBA LabRAM HR Evolution with a CCD detector using a visible laser (λ = 532 nm) and UV laser (λ = 325 nm) with an output laser power of 5 mW. The scanning scope of the visible and UV Raman spectra were 300–700 cm^{-1}. The scanning scope of the in situ visible Raman spectra were 200–750 cm^{-1} and in situ UV Raman spectra were 300–1800 cm^{-1}. Before the in situ Raman test, 30 mg of model soot and 270 mg of catalysts powder were mixed and milled carefully by an agate mortar for 2 min for "loose contact" conditions. During the in situ Raman test, the mixture was heated from 30 °C to 500 °C at a heating rate of 10 °C min^{-1} then back to 30 °C at a cooling rate of 20 °C min^{-1} under 10% O_2/Ar in an in-situ reaction tank. And the in situ Raman spectra were achieved at every 100 °C.

3. Results and discussion

3.1. Repeated soot reaction activity tests

Our previous works found that the $MnO_x(0.4)$-CeO_2 exhibited the highest catalytic activity among a series of MnO_x-CeO_2 catalysts with various Mn/Ce molar ratios, due to their highest surface area and oxygen vacancies concentration [38]. However, the durability of catalytic activity was still essential so that TPO was used to evaluate the catalytic activity toward repeated soot oxidation. Fig. 1 shows the TPO curves of fresh and reused $MnO_x(0.4)$-CeO_2 samples for soot oxidation under loose contact conditions, and the results are listed in Table 1.

As shown in Fig. 1, TPO curves of reused samples shift a little to higher temperature zones by comparing with the sample in TPO 1st, the first soot oxidation process, but they almost overlap. According to Table 1, the T_i obtained from TPO 1st is 285.5 °C, while it increases slightly to 300.7 °C in TPO 2nd, the second soot oxidation process, and almost keeps at a relatively stable temperature in TPO 3rd, the third TPO period. Analogously, the T_m over the reused samples follow the same pattern as T_i. The T_i and T_m ascend mildly after the first soot oxidation, signifying the slight decline of activity of reused catalysts, which implies that the $MnO_x(0.4)$-CeO_2 is highly active and stable for repeated soot oxidation. However, the relatively light degrading phenomenon catches our attention. It is reasonable to assume that some irreversible changes of structure of $MnO_x(0.4)$-CeO_2 occur in the first utilization, which are crucial in maintaining the satisfactory activity.
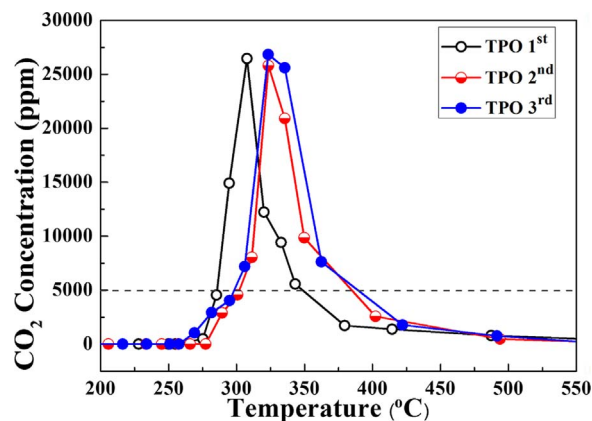

Fig. 1. TPO profile of fresh and reused $MnO_x(0.4)$-CeO_2 catalysts for soot oxidation under loose contact conditions.

Table 1
Soot oxidation activity of the fresh and reused $MnO_x(0.4)$-CeO_2 catalysts under loose contact conditions.

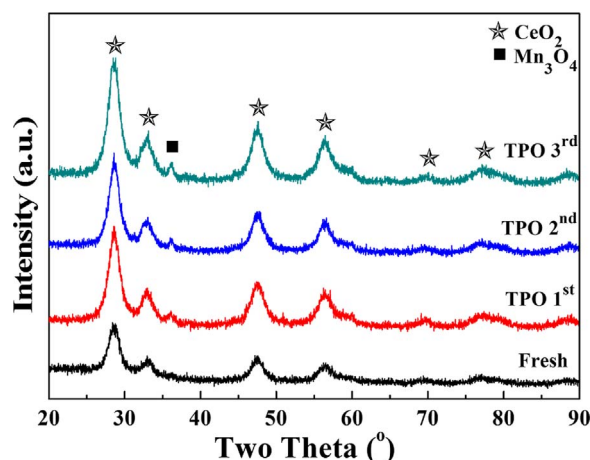| Reaction cycle	T_i/°C	T_m/°C	T_c/°C	ΔT/°C
TPO 1st	285.5	307.7	414.3	128.8
TPO 2nd	300.7	323.5	474.8	174.1
TPO 3rd	300.4	323.3	475.7	175.3

Fig. 2. X-ray diffraction patterns of $MnO_x(0.4)$-CeO_2 catalysts before and after TPO.

3.2. Catalyst characterization

3.2.1. Structural characterization

Fig. 2 is the XRD patterns of fresh and reused $MnO_x(0.4)$-CeO_2 catalysts. The fresh $MnO_x(0.4)$-CeO_2 sample is dominated by the ceria characteristic peaks with the cubic fluorite structure, and no manganese species characteristic peaks are detected. This observation suggests that the manganese species might enter into the fluorite structure of ceria to form Mn-Ce-O solid solution or the manganese species have well dispersed on ceria surface [30,39,40].

For the reused samples, the XRD patterns mainly show the ceria characteristic peaks, with weak diffraction peaks of Mn_3O_4, implying the major structure of catalysts is unchanged during the reaction process. However, comparing with fresh sample, the intensity of CeO_2 diffraction peaks becomes stronger, indicating that the spent samples have been sintered after the first soot oxidation process. Meanwhile, the emergence of Mn_3O_4 diffraction peaks can be attributed to the Mn_3O_4 segregated from the ceria lattice irreversibly. Minority of manganese species separated from the Mn-Ce-O solid solution and formed Mn_3O_4 crystal phase on the catalysts surface will enhance the crystallite size as well as lower the surface area, followed by the reduction of active surface species and oxygen vacancies [30,41]. All of these effects result in the slight decline of catalytic activity for soot oxidation, as shown in the TPO results.

The BET surface areas are listed in Table 2. The results show that a high value of $89.08\,m^2\,g^{-1}$ is obtained for the fresh $MnO_x(0.4)$-CeO_2 catalyst and the surface area decreases after the first utilization. Interestingly, it can be observed that the BET surface areas tend to be stable

Table 2
Specific surface area of fresh and reused $MnO_x(0.4)$-CeO_2 catalysts.

Reaction cycle	Specific surface area/($m^2\,g^{-1}$)
Fresh	89.08
1st Cycle	58.07
2nd Cycle	55.25
3rd Cycle	52.58

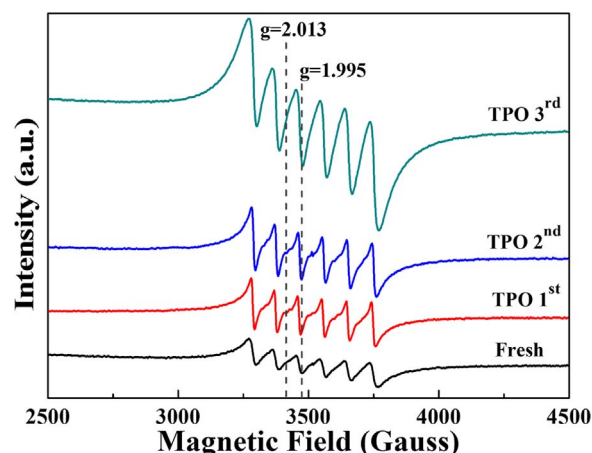**Fig. 3.** Electron paramagnetic resonance spectra of fresh and reused $MnO_x(0.4)$-CeO_2 catalysts at X-band (9.87 GHz), room temperature.

among the reused samples. The BET results are in good accordance with the degrading phenomenon revealed by TPO measurement.

3.2.2. EPR

The electron paramagnetic resonance is employed to identify the manganese and oxygen species in fresh and reused $MnO_x(0.4)$-CeO_2 catalysts. Fig. 3 shows the EPR spectra measured at the room temperature for fresh and reused samples. The g factor is calculated by the X-band frequency and magnetic field values. Both the fresh and reused catalysts exhibit intense six hyperfine lines with the central g factor at 1.995 and the average hyperfine coupling constant A at 91 G, which can be ascribed to Mn^{2+} ions [30,41,42]. The intensity of EPR line reflects the Mn^{2+} ions concentration in the catalyst and it notably enhances after the first utilization, which probably implies the partial reduction of manganese species resulting in the concentration of Mn^{2+} ions increases. However, the superoxide species (O_2^-), which exhibit a hyperfine line with the g factor at 2.013 and the hyperfine coupling constant A at 75 G [43,44], are unobservable in Mn doped ceria catalysts. The g factor of superoxide species is almost close to Mn^{2+} ions as well as the less A value for superoxide species. Therefore, the undetected O_2^- species signals are possibly caused by the overlapping by the six hyperfine lines. In general, EPR measurements demonstrate that the amount of Mn^{2+} increases at the repeated soot oxidation which is attributed to the irreversible conversion of manganese species from high oxidation state to low oxidation state.

3.2.3. XPS

The oxidation states of surface species from fresh and spent $MnO_x(0.4)$-CeO_2 catalysts could be detected by XPS analysis. For this purpose, the XPS spectra of Ce 3d, Mn 2p and O 1 s for fresh and reused samples are shown in Figs. 4–6 respectively, and the compositions of surface species are listed in Table 3. From the Ce 3d spectra, it is known to be complicated due to the existence of two different cerium oxidation states [41,45]. With the purpose of identifying the specific oxidation state of cerium ions, the label u and v peaks are assigned to $3d_{3/2}$ and $3d_{5/2}$ spin orbit component, respectively. The peaks labelled as v, v_2, v_3, u, u_2 and u_3 are characteristic peaks of Ce^{4+}, and the other two peaks labelled as v_1 and u_1 are related to Ce^{3+} [46,47]. As is demonstrated in Table 3, the fresh sample exhibits the highest Ce^{4+}/Ce^{3+} ratio of 4.48, whereas the reacted ones only have 2.88-3.58. In our previous work, the redox couple of Ce^{4+}/Ce^{3+} plays the active species role in soot oxidation, which the transformation from Ce^{4+} to Ce^{3+} could create more Frenkel-type oxygen vacancies that are beneficial for activation of surface oxygen species [38]. Thus it can be seen that the better catalytic activity in the first reaction due to partial Ce^{4+} irreversible transfers to Ce^{3+} with the active oxygen species releasing.
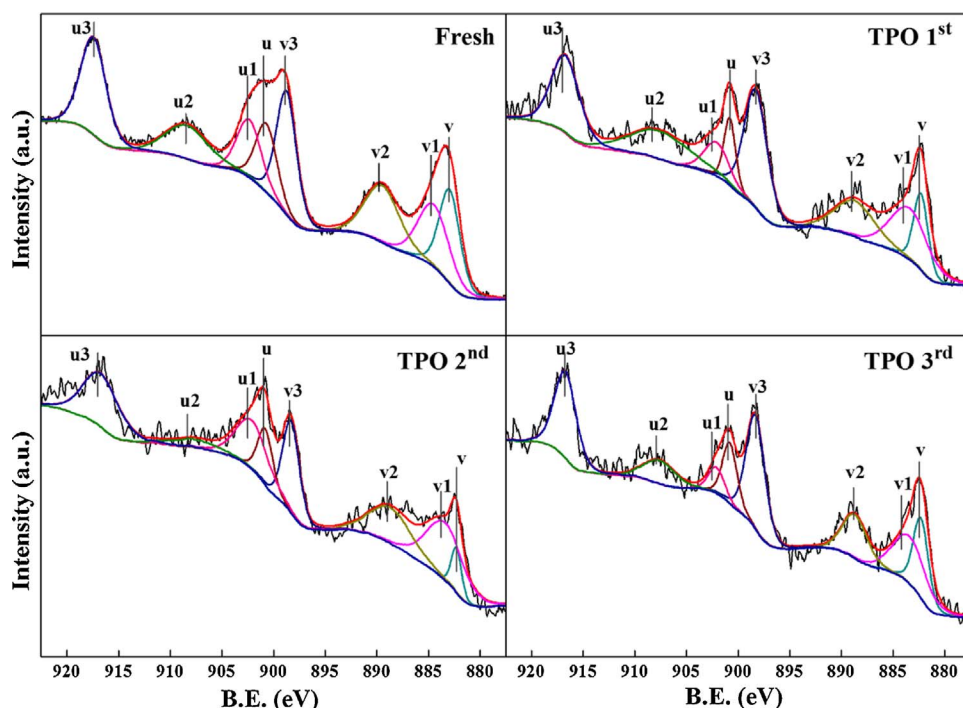
Fig. 4. Ce 3d core level XPS spectra of fresh and re-used $MnO_x(0.4)$-CeO_2 catalysts.

Fig. 5 shows the Mn 2p spectra, the observed binding energies at around 643–644 eV and 641–642 eV can be attributed to Mn^{4+} and Mn^{3+} (or Mn^{2+}) species respectively [41,48], which suggests the co-existence of three kinds of Mn species (Mn^{2+}, Mn^{3+} and Mn^{4+}) on the catalysts surface. The $Mn^{4+}/(Mn^{3+} + Mn^{2+})$ ratio shown in Table 3 decreases from 1.75 (fresh sample) to 0.85-1.28 (reacted one), indicating the partially irreversible transformation of manganese species from high oxidation state (+4) to low oxidation states (+2 and +3) and the formation of Mn_3O_4 crystal phase, as proved by XRD and EPR spectra. Specifically, the manganese species change from highly dispersion to aggregation could also answer for the mildly gradual decline of the catalytic activity in repeated application.

As for surface oxygen species, it can be observed from the O 1 s spectra that three peaks at about 529–530 eV, 530–532 eV and 533–534 eV are characteristic of lattice oxygen (O_{latt}), surface oxygen (O_{sur}) and adsorbed oxygen (O_{ads}), respectively [49,50]. The concentration of three kinds of oxygen species is calculated by integrating peak areas of the O 1 s spectra and the values are shown in Table 3. The results show that O_{latt} slightly decreases after the fresh utilization while O_{sur} increases. Interestingly, the proportion of three kinds of oxygen species reaches to a stable condition in the reused sample tests. We suppose that O_{latt} migrates to catalysts surface and reacts with soot as active oxygen species, which results in the reduction of O_{latt} concentration. Meanwhile, catalysts form O_{ads} by adsorbing gas phase O_2
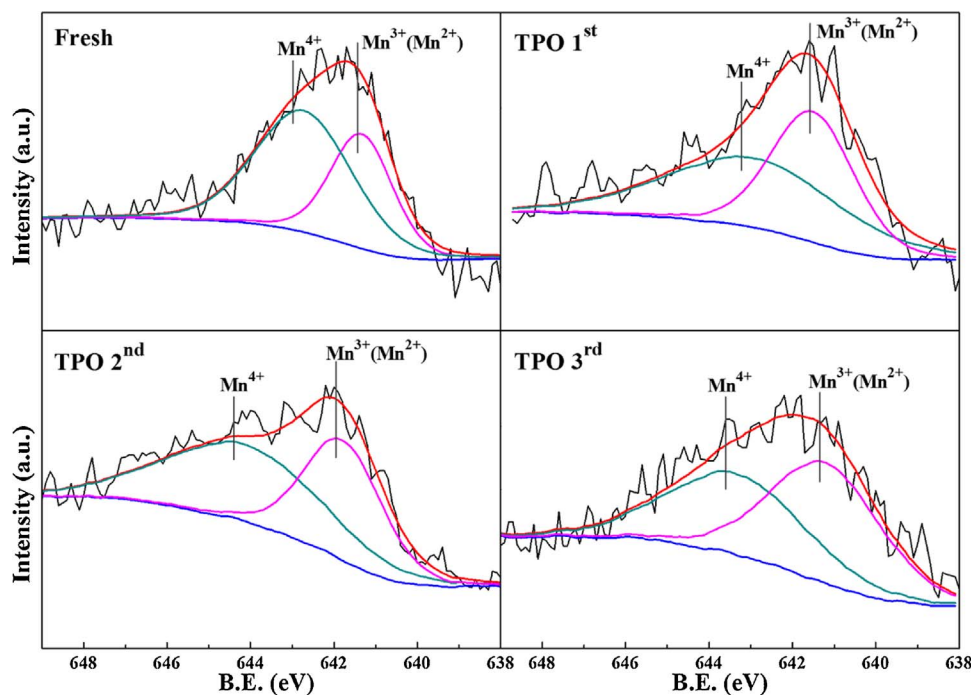

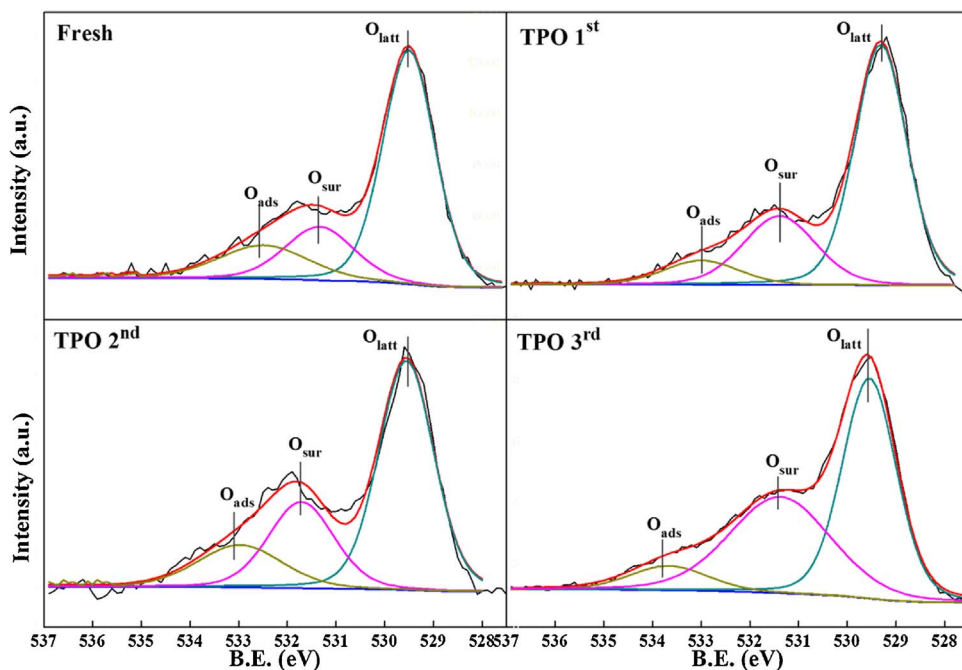**Fig. 5.** Mn 2p core level XPS spectra of fresh and reused $MnO_x(0.4)$-CeO_2 catalysts.

Fig. 6. O 1 s core level spectra of fresh and reused MnO$_x$(0.4)-CeO$_2$ catalysts.

Table 3
Amount of surface species from fresh and reused MnO$_x$(0.4)-CeO$_2$ catalysts based on XPS analysis.

Reaction cycle	O/at.%			Ce^{4+}/Ce^{3+}	Mn^{4+}/(Mn^{2+} + Mn^{3+})
	O$_{ads}$	O$_{sur}$	O$_{latt}$		
Fresh	20.37	23.93	55.70	4.48	1.75
1st Cycle	21.22	30.53	48.25	3.58	1.11
2nd Cycle	21.03	33.31	45.66	2.88	0.85
3rd Cycle	20.09	32.28	47.63	3.21	1.28

molecules to supplement the consumed lattice oxygen through the following path: O$_2$ → O$_{ads}$ → O$_{sur}$ → O$_{latt}$. However, after the first soot oxidation process, the O$_{latt}$ cannot be fully recovered due to the fact that the catalyst structure suffers irreversible transformation in the first reaction cycle, which probably depresses the catalytic performance.

3.2.4. Raman spectra

Fig. 7 shows the visible and UV Raman spectra of fresh and reused MnO$_x$(0.4)-CeO$_2$ catalysts. Both the fresh and reused samples show a strong Raman peak at 465 cm^{-1} in the visible Raman spectra which is due to the characteristic vibration of the F$_{2g}$ mode of the CeO$_2$ fluorite-like structure [51,52]. Comparing with the fresh one, the F$_{2g}$ peak of reacted samples becomes sharper attributed to the increase of crystal size, caused by the sintering and aggregation [41]. Moreover, the emergence of Mn$_3$O$_4$ characteristic peak at about 650 cm^{-1} indicates the segregation of partial manganese species from ceria lattice and formation of independent Mn$_3$O$_4$ crystal phase after the first utilization [31,53]. However, the intensity of the Mn$_3$O$_4$ characteristic peak keeps stable after the second and third reaction cycle, implying that the separation of manganese species and formation of Mn$_3$O$_4$ crystal phase occur irreversibly in the first reaction cycle. These are highly consistent with the XRD detection.

The resonance Raman effect enhances Raman signal when the Raman scattering light is excited by UV laser [54,55]. As a result, UV Raman is more sensitive to defect sites in ceria than visible Raman, so that it can effectively observe defect sites including oxygen vacancies [54,56].
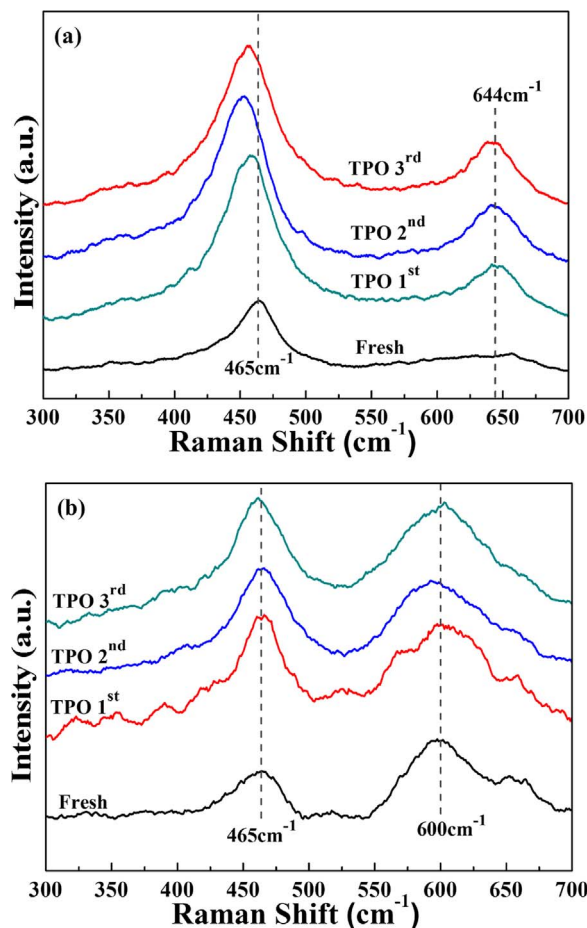

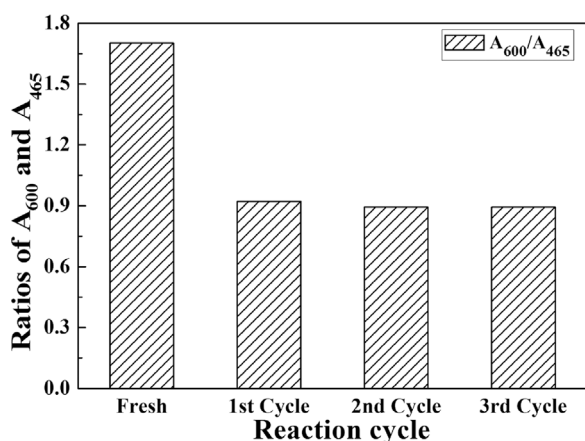**Fig. 7.** Visible (λ = 532 nm) (a) and UV (λ = 325 nm) (b) Raman spectra of fresh and reused MnO$_x$(0.4)-CeO$_2$ catalysts.

Fig. 8. Oxygen vacancies concentrations of fresh and reused $MnO_x(0.4)$-CeO_2 catalysts.

From the UV Raman spectra, characteristic peaks at 600 cm^{-1} are ascribed to interstitial (Frenkel-type) oxygen vacancy [56,57]. The Raman peak areas ratio of the Frenkel-type oxygen vacancies peak at 600 cm^{-1} and the F_{2g} peak at 465 cm^{-1}, which is denoted as A_{600}/A_{465}, can reflects the concentration of oxygen vacancies [58]. The A_{600}/A_{465} ratios for fresh sample and reused sample are shown in Fig. 8. It is observed that the concentration of Frenkel-type oxygen vacancies approximately reduces by a half after the first reaction cycle, and reaches to a stable condition after the second and third cycle. Therefore, it is probable that part of oxygen vacancies suffer irreversible transformations during the first soot reaction cycle, which is mainly attributed to the separation of manganese species from ceria crystal lattice that is confirmed by XRD and visible Raman. Those irreversible consumptions of oxygen vacancies mainly cause the deactivation of $MnO_x(0.4)$-CeO_2 catalysts after the first utilization. However, it is surprising that the catalytic activity slightly decreases with the Frenkel-type oxygen vacancies concentrations decline remarkably, combining the TPO and UV Raman results. This intriguing observation is reasonably because the spectators occupy the major of irreversibly consumed oxygen vacancies, which will be confirmed by the in situ Raman.

In situ visible Raman spectra of mixture of fresh catalysts and soot under 10% O_2/Ar shown in Fig. 9 give information on the structural changes on $MnO_x(0.4)$-CeO_2 catalysts. From the spectra, the main peak at around 465 cm^{-1} always dominates during the whole reaction stage, which means that the catalysts maintain the major fluorite-like structure. Clearly, Mn_3O_4 characteristic peak at 650 cm^{-1} occurs when the
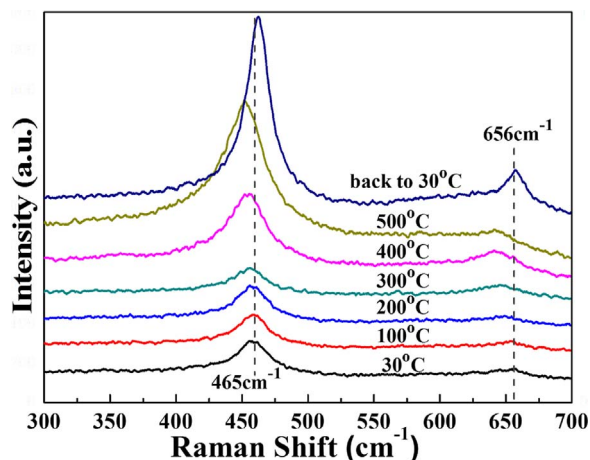

Fig. 9. In situ visible ($\lambda = 532$ nm) Raman spectra of mixture of soot and fresh $MnO_x(0.4)$-CeO_2 catalysts at different temperature under 10% O_2/Ar.
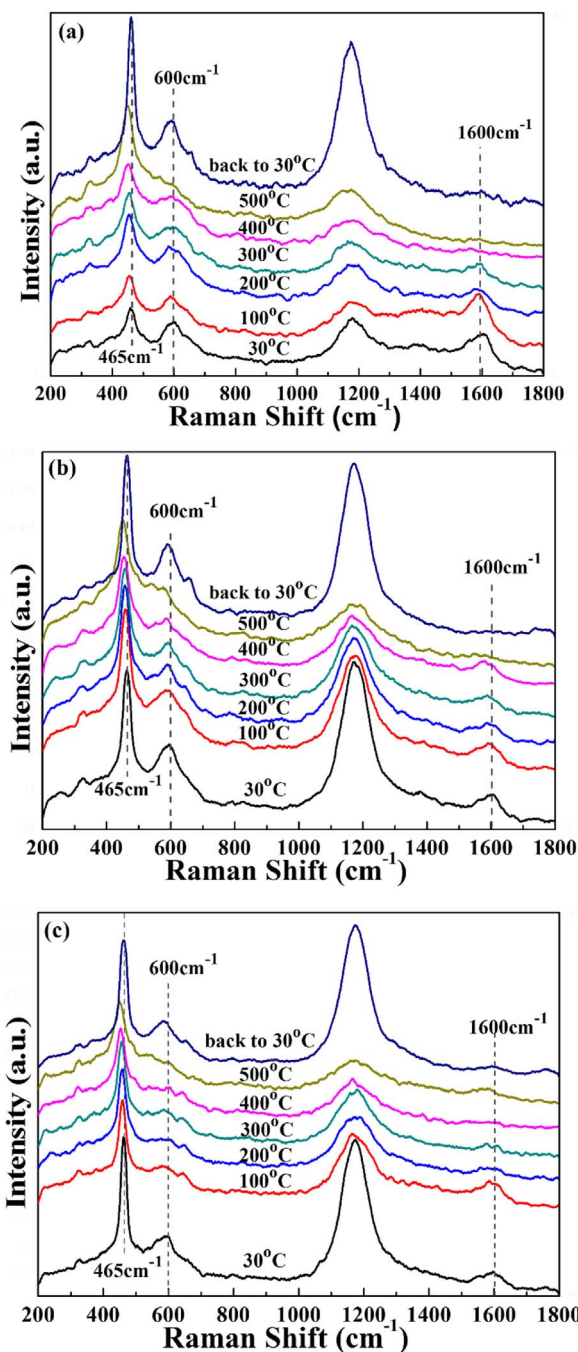

Fig. 10. In situ UV Raman ($\lambda = 325$ nm) Raman spectra of mixture of soot and $MnO_x(0.4)$-CeO_2 catalysts under 10% O_2/Ar during the first cycle (a), second cycle (b) and third cycle (c).

temperature cools down to 30 °C, which is in good agreement with the separation of manganese species after the first reaction, as proved by XRD. However, it is difficult to observe the change of oxygen vacancies concentration during the soot oxidation process due to the weak oxygen vacancies signal in visible Raman.

In situ UV Raman spectra of mixture of catalysts and soot with three reaction cycles are displayed in Fig. 10. The UV Raman spectra are composed of a main F_{2g} peak at 465 cm^{-1} and several other characteristic peaks at 600 cm^{-1}, 1179 cm^{-1} and 1600 cm^{-1} which are attributed to the Frenkel-type oxygen vacancies [56,57], second-order longitudinal optical [56] and soot [59], respectively. The position of F_{2g} peak slightly shifts toward lower wavenumber with the reaction
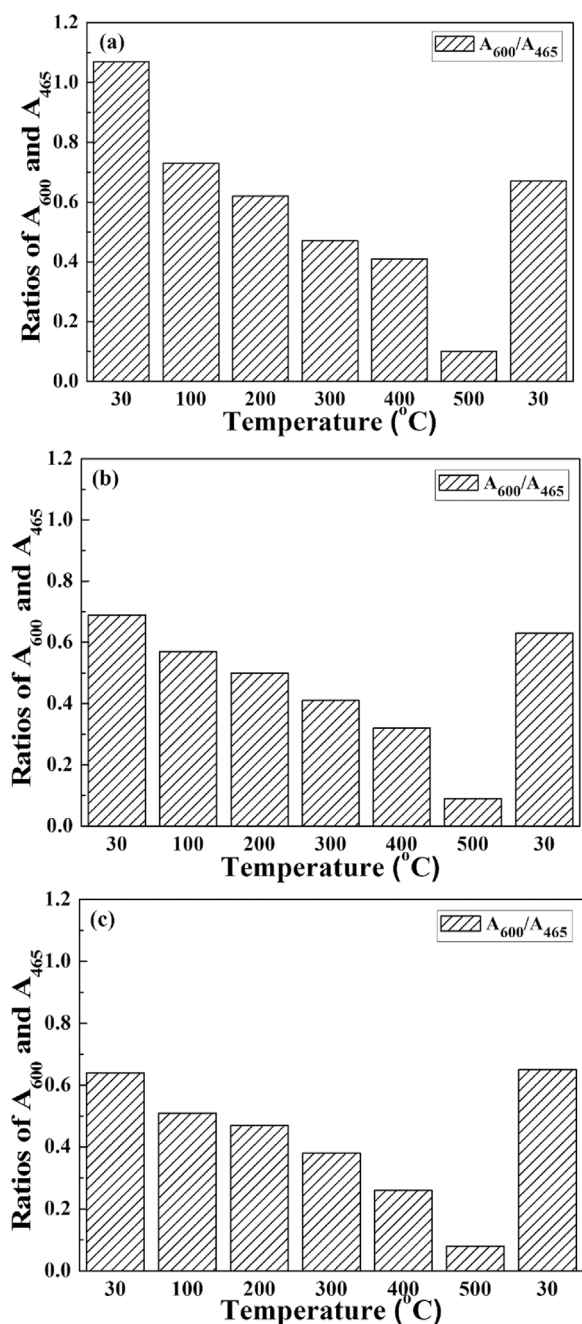
Fig. 12. Concentrations of spectator and participator of Frenkel-type oxygen vacancies in different reaction periods.

Fig. 11. Oxygen vacancies concentration conversion of $MnO_x(0.4)$-CeO_2 catalysts during the first cycle (a), second cycle (b) and third cycle (c).

reaction. Fig. 11 shows the conversion of A_{600}/A_{465} at different temperatures. Obviously, the oxygen vacancies go through both consumed and regenerated periods, during the three soot oxidation process. For each reaction cycle, the Frenkel-type oxygen vacancies have two existing forms, spectators and participators. The consumptions of oxygen vacancies at low temperature region (from room temperature to 250 °C), corresponding the soot heating process, are defined as spectators which are hardly work on oxidizing soot. And the consumptions of oxygen vacancies at high temperature region (above 300 °C), corresponding the soot reaction process, are defined as participators which are play an important role in soot oxidation. Fig. 12 shows the concentration of spectators and participators in different soot oxidation period. The concentration of spectators decreases more than a half by comparing the first cycle with the second and third cycle. Meanwhile, the participators merely decline a little. Thus, Frenkel-type oxygen vacancies significantly decline after the first soot oxidation, observed by UV Raman, which is probably attributed to the remarkable reduction of spectators.

The generation of spectator is probably due to the deviation of O_{latt} from the original position at low temperature region. However, as for participator, it is probably formed when O_{latt} escapes from the lattice and reacts with soot as active oxygen species at high temperature region. Interestingly, Fig. 12 and Table 3 show that both the participator and O_{latt} slightly decrease after the first cycle and the decrement percentage of participator and O_{latt} is similarly (about 12%), which implies that participator can reflect the amount of activable O_{latt}. Therefore, the majority of participators exist in both fresh and reused catalysts ensuring the satisfactory activity and stability for repeated soot oxidation.

3.2.5. Influential factors of activity

Fig. 13 shows the surface active species and oxygen vacancies transformations in the different reaction cycles. Both the Frenkel-type oxygen vacancies concentrations and the surface active species (lattice oxygen and Mn^{4+}) follow the similar variation trend. Concretely, the amount of surface active species and oxygen vacancies concentration decline after the first soot reaction. Correspondingly, the maximum combustion rate temperature rises a little after the first cycle, representing the catalytic activity slightly declines in the repeated reaction periods. These results directly reflect the negative correlation between the key surface species as well as oxygen vacancies and the catalytic activity. It is helpful to demonstrate that the deactivation of $MnO_x(0.4)$-CeO_2 catalysts is associated with the reduction of the surface active species and Frenkel-type oxygen vacancies due to the irreversible manganese phase separation in catalyst structure. The transformation

temperature increasing from room temperature to 500 °C, which is due to thermal expansion as well as phonon confinement [56,57]. The intensity of soot peaks at 1600 cm^{-1} begin to decline at 300 °C and almost disappear at 400–500 °C reflecting that soot is ignited at about 300 °C and burnt out at 400–500 °C, which is well consistent with the TPO results. The intensity of Frenkel-type oxygen vacancies gradually weakens when the temperature increases. Especially, the signal of Frenkel-type oxygen vacancies is almost undetectable at 400–500 °C, but it reappears while the temperature returns to 30 °C. This transformation of oxygen vacancies proves that oxygen vacancies are consumed when the soot is combusted and are partly regenerated after reaction.

The area ratios of Frenkel-type oxygen vacancies peak and F_{2g} peak from in situ UV Raman reflect the oxygen vacancies concentration at different reaction temperatures, which helps us to find out the spectators and participators of Frenkel-type oxygen vacancies in the soot
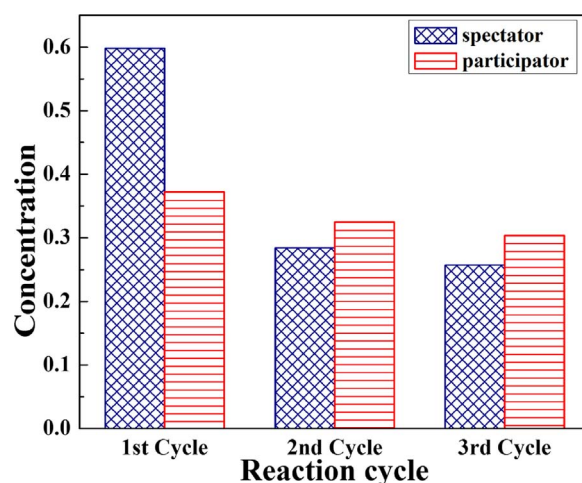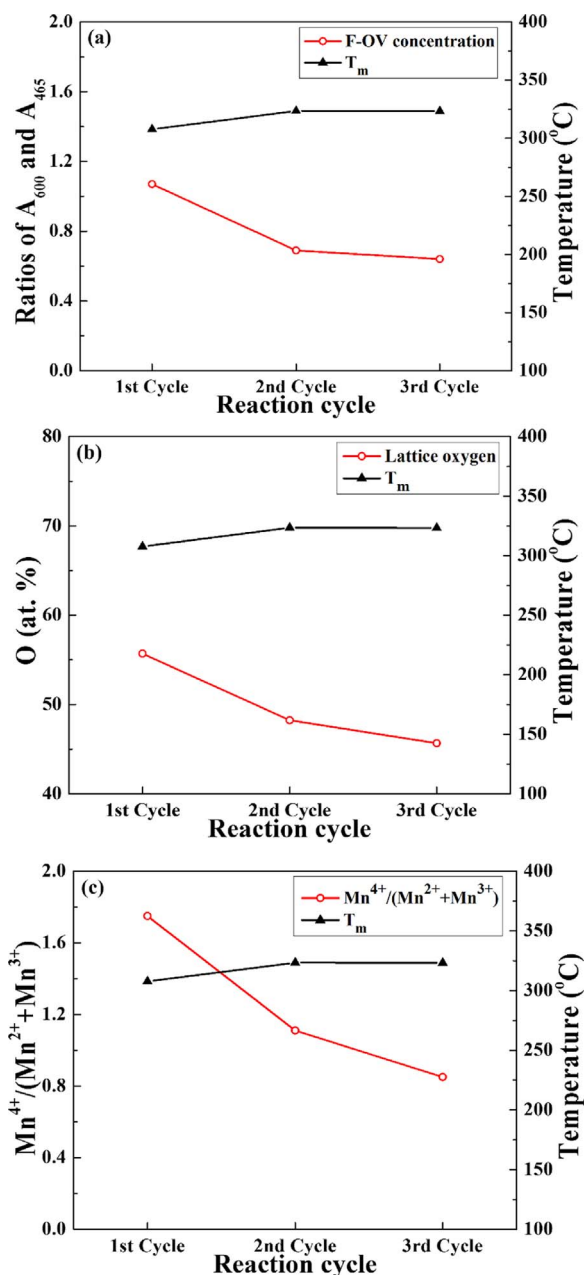
Fig. 13. The relationship between soot catalytic activity and oxygen vacancies concentration (a), lattice oxygen (b) and $Mn^{4+}/(Mn^{2+} + Mn^{3+})$ (c) during the repeated soot oxidation.

Fig. 14. The correlation between catalytic activity and participator, and the relationship between catalytic activity and spectator.

4. Conclusions

To summarize, $MnO_x(0.4)$-CeO_2 catalysts prepared by the citric acid complex method are repeatedly employed for soot oxidation. Three cycles of soot reaction active test under 10% O_2/Ar indicate that the $MnO_x(0.4)$-CeO_2 catalysts possess favorable activity and satisfactory durability toward soot oxidation. Comparing with fresh catalysts, the separations of active manganese species as well as the irreversible consumptions of oxygen vacancies and lattice oxygen are detected in reused ones, which respond to the depression in the catalytic activity. However, the spectators probably exist in Frenkel-type oxygen vacancies which are hardly work on oxidizing soot. In addition, majority of participators regenerate after soot oxidation process according to in situ UV Raman, ensuring the ability to activate O_{latt} during repeated utilization, which is crucial in maintaining the favorable activity and satisfactory durability.

Acknowledgements

References

[1] Q. Shen, G. Lu, C. Du, Y. Guo, Y. Wang, Y. Gou, et al., Role and reduction of NO_x in the catalytic combustion of soot over iron-ceria mixed oxide catalyst, Chem. Eng. J. 218 (2013) 164–172.

[2] X. Wu, F. Lin, H. Xu, D. Weng, Effects of adsorbed and gaseous NO_x species on catalytic oxidation of diesel soot with MnO_x-CeO_2 mixed oxides, Appl. Catal. B: Environ. 96 (2010) 101–109.

[3] C.B. Lim, H. Kusaba, H. Einaga, Y. Teraoka, Catalytic performance of supported precious metal catalysts for the combustion of diesel particulate matter, Catal. Today 175 (2011) 106–111.

[4] Q. Li, M. Meng, F. Dai, Y. Zha, Y. Xie, T. Hu, et al., Multifunctional hydrotalcite-derived K/MnMgAlO catalysts used for soot combustion, NO_x storage and simultaneous soot-NO_x removal, Chem. Eng. J. 184 (2012) 106–112.

[5] D.M. Brown, M.R. Wilson, W. Macnee, V. Stone, K. Donaldson, Size-dependent proinflammatory effects of ultrafine polystyrene particles: a role for surface area and oxidative stress in the enhanced activity of ultrafines, Toxicol. Appl. Pharm. 175 (2001) 191–199.

[6] P.A. Kumar, M.D. Tanwar, S. Bensaid, N. Russo, D. Fino, Soot combustion improvement in diesel particulate filters catalyzed with ceria nanofibers, Chem. Eng. J. 207 (2012) 258–266.

[7] N. Russo, D. Fino, G. Saracco, V. Specchia, Promotion effect of Au on perovskite catalysts for the regeneration of diesel particulate filters, Catal. Today 137 (2008) 306–311.

of spectators and participators in different reaction periods is shown in Fig. 14. Clearly, the spectators reduce by a half after the first reaction, which trend is similar to the reduction of Frenkel-type oxygen vacancies. This result suggests that the spectators occupy the majority of consumed oxygen vacancies, which merely exert a slight influence on catalytic activity. In contrast, the participators, which reflect the amount of activable O_{latt}, only show a slight decrease. The stable level of participator ensures the ability to activate O_{latt} during repeated utilization, which is crucial in soot oxidation. Therefore, the $MnO_x(0.4)$-CeO_2 catalysts show favorable activity and satisfactory durability toward soot oxidation.
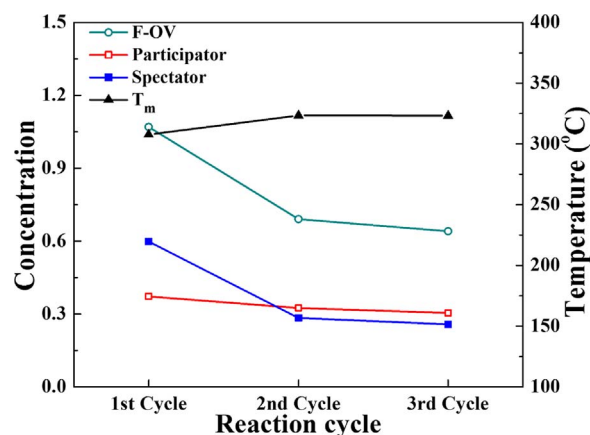
[8] I. Atribak, A. Bueno-Lopez, A. Garcia-Garcia, Thermally stable ceria-zirconia catalysts for soot oxidation by O_2, Catal. Commun. 9 (2008) 250–255.

[9] M. Machida, Y. Murata, K. Kishikawa, D. Zhang, K. Ikeue, On the reasons for high activity of CeO_2 catalyst for soot oxidation, Chem. Mater. 20 (2008) 4489–4494.

[10] M. Machida, D. Kurogi, T. Kijima, MnO_x-CeO_2 binary oxides for catalytic NO_x-sorption at low temperatures. Selective reduction of sorbed NO_x, Chem. Mater. 12 (2000) 3165–3170.

[11] L.E. Gomez, J.F. Munera, B.M. Sollier, E.E. Miro, A.V. Boix, Raman in situ characterization of the species present in Co/CeO_2 and Co/ZrO_2 catalysts during the $COProx$ reaction, Int. J. Hydrogen Energy 41 (2016) 4993–5002.

[12] X. Liu, J. Lu, K. Qian, W. Huang, M. Luo, A comparative study of formaldehyde and carbon monoxide complete oxidation on MnO_x-CeO_2 catalysts, J. Rare Earths 27 (2009) 418–424.

[13] N. Zouaoui, M. Issa, D. Kehrli, M. Jeguirim, CeO_2 catalytic activity for soot oxidation under NO/O_2 in loose and tight contact, Catal. Today 189 (2012) 65–69.

[14] K. Krishna, A. Bueno-Lopez, M. Makke, J.A. Moulijn, Potential rare earth modified CeO_2 catalysts for soot oxidation: i. Characterisation and catalytic activity with O_2, Appl. Catal. B: Environ. 75 (2007) 189–200.

[15] A. Setiabudi, J. Chen, G. Mul, M. Makkee, J.A. Moulijn, CeO_2 caralysed soot oxidation: the role of active oxygen to accelerate the oxidation conversion, Appl. Catal. B: Environ. 51 (2004) 9–19.

[16] D. Fino, N. Russo, G. Saracco, V. Specchia, The role of superficial oxygen in some perovskites for the catalytic combustion of soot, J. Catal. 217 (2003) 367–375.

[17] A. Bueno-Lopez, K. Krishna, B. van der Linden, G. Mul, J.A. Moulijn, M. Makkee, On the mechanism of model diesel soot-O_2 reaction catalyzed by Pt-containing La^{3+}-doped CeO_2: A TAP study with isotopic O_2, Catal. Today 121 (2007) 237–245.

[18] H. Muroyama, S. Hano, T. Matsui, K. Eguchi, Catalytic soot combustion over CeO_2-based oxides, Catal. Today 153 (2010) 133–135.

[19] J. Liu, Z. Zhao, J. Wang, C. Xu, A. Duan, G. Jiang, et al., The highly active catalysts of nanometric CeO_2-supported cobalt oxides for soot combustion, Appl. Catal. B: Environ. 84 (2008) 185–195.

[20] X. Li, S. Wei, Z. Zhang, Y. Zhang, Z. Wang, Q. Su, et al., Quantification of the active site density and turnover frequency for soot combustion with O_2 on Cr doped CeO_2, Catal. Today 175 (2011) 112–116.

[21] H. Bao, X. Chen, J. Fang, Z. Jiang, W. Huang, Structure-activity relation of Fe_2O_3-CeO_2 composite catalysts in CO oxidation, Catal. Lett. 125 (2008) 160–167.

[22] P. Singh, M.S. Hegde, Controlled synthesis of nanocrystalline CeO_2 and $Ce_{1-x}M_xO_2$-$(M = Zr, Y, Pr and Fe)$ solid solutions by the hydrothermal method: structure and oxygen storage capacity, J. Solid State Chem. 181 (2008) 3248–3256.

[23] M. Fu, X. Yue, D. Ye, J. Ouyang, B. Huang, J. Wu, et al., Soot oxidation via CuO doped CeO_2 catalysts prepared using coprecipitation and citrate acid complex-combustion synthesis, Catal. Today 153 (2010) 125–132.

[24] M.E. Becerra, N.P. Arias, O.H. Giraldo, F.E. Lopez Suarez, M.J. Illan Gomez, A. Bueno Lopez, Soot combustion manganese catalysts prepared by thermal decomposition of $KMnO_4$, Appl. Catal. B: Environ. 102 (2011) 260–266.

[25] V.P. Santos, M.F.R. Pereira, J.J.M. Orfao, J.L. Figueiredo, The role of lattice oxygen on the activity of manganese oxides towards the oxidation of volatile organic compounds, Appl. Catal. B: Environ. 99 (2010) 353–363.

[26] S.S.T. Bastos, J.J.M. Orfao, M.M.A. Freitas, M.F.R. Pereira, J.L. Figueiredo, Manganese oxide catalysts synthesized by exotemplating for the total oxidation of ethanol, Appl. Catal. B: Environ. 93 (2010) 30–37.

[27] D. Mukherjee, B.G. Rao, B.M. Reddy, CO and soot oxidation activity of doped ceria: influence of dopants, Appl. Catal. B: Environ. 197 (2016) 105–115.

[28] Q. Liang, X. Wu, D. Weng, H. Xu, Oxygen activation on Cu/Mn-Ce mixed oxides and the role in diesel soot oxidation, Catal. Today 139 (2008) 113–118.

[29] K. Tikhomirov, O. Krocher, M. Elsener, A. Wokaun, MnO_x-CeO_2 mixed oxides for the low-temperature oxidation of diesel soot, Appl. Catal. B: Environ. 64 (2006) 72–78.

[30] M.M. Fiuk, A. Adamski, Activity of MnO_x-CeO_2 catalysts in combustion of low concentrated methane, Catal. Today 257 (2015) 131–135.

[31] B. Fazio, L. Spadaro, G. Trunfio, J. Negro, F. Arena, Raman scattering of MnO_x-CeO_x composite catalysts: structural aspects and laser-heating effects, J. Raman Spectrosc. 42 (2011) 1583–1588.

[32] Z. Wang, G. Shen, J. Li, H. Liu, Q. Wang, Y. Chen, Catalytic removal of benzene over CeO_2-MnO_x composite oxides prepared by hydrothermal method, Appl. Catal. B: Environ. 138–139 (2013) 253–259.

[33] M. Dhakad, T. Mitsuhashi, S. Rayalu, P. Doggali, S. Bakardjiva, J. Subrt, et al., Co_3O_4-CeO_2 mixed oxides-based catalytic materials for diesel soot oxidation, Catal. Today 132 (2008) 188–193.

[34] N. Zouaoui, M. Issa, D. Kehrli, M. Jeguirim, CeO_2 catalytic activity for soot oxidation under NO/O_2 in loose and tight contact, Catal. Today 189 (2012) 65–69.

[35] C. Su, P.J. Mcginn, The effect of Ca^{2+} and Al^{3+} additions on the stability of

[36] X. Zhu, X. Gao, R. Qin, Y. Zeng, R. Qu, C. Zheng, Plasma-catalytic removal of formaldehyde over Cu-Ce catalysts in a dielectric barrier discharge reactor, Appl. Catal. B: Environ. 170–171 (2015) 293–300.

[37] X. Yue, X. Zhang, M. Fu, B. Huang, H. Liang, D. Ye, Effect of SO_2 on soot oxidation over $La_{0.8}K_{0.2}Cu_{0.05}Mn_{0.95}O_3$ perovskites-type catalyst, Chin. J. Inorg. Chem. 25 (2009) 1170–1176.

[38] M. Zhang, M. Fu, J. Wu, B. Huang, H. Liang, D. Ye, Characteristic of surface oxygen species and catalytic property on MnO_x-CeO_2 for soot combustion, J. Chin. Soc. Rare Earth 29 (2011) 303–309.

[39] X. Wu, S. Liu, D. Weng, F. Lin, R. Ran, MnO_x-CeO_2-Al_2O_3 mixed oxides for soot oxidation: activity and thermal stability, J. Hazard. Mater. 187 (2011) 283–290.

[40] T. Akashi, S. Sato, R. Takahashi, T. Sodesawa, K. Inui, Catalytic vapor-phase cyclization of 1,6-hexanediol into cyclopentanone, Catal. Commun. 4 (2003) 411–416.

[41] P. Venkataswamy, K.N. Rao, D. Jampaiah, B.M. Reddy, Nanostructured manganese doped ceria solid solution foe CO oxidation at lower temperature, Appl. Catal. B: Environ. 162 (2015) 122–132.

[42] B. Murugan, A.V. Ramaswamy, Chemical states and redox properties of Mn/CeO_2-TiO_2 nanocomposites prepared by solution combustion route, J. Phys. Chem. C 112 (2008) 20429–20442.

[43] A. Aboukais, S. Aouad, M. Skaf, S. Hany, M. Labaki, R. Cousin, EPR investigation of the nature of oxygen species present on the surface of gold impregnated cerium oxide, Mater. Chem. Phys. 170 (2016) 285–293.

[44] M. Machida, Y. Murata, K. Kishikawa, D. Zhang, K. Ikeue, On the reasons for high activity of CeO_2 catalyst for soot oxidation, Chem. Mater. 20 (2008) 4489–4494.

[45] B. Guan, H. Lin, L. Zhu, Z. Huang, Selective catalytic reduction of NO_x with NH_3 over Mn, Ce substitution $Ti_{0.9}V_{0.1}O_{2-8}$ nanocomposites catalysts prepared by self-Propagating high-Temperature synthesis method, J. Phys. Chem. C 115 (2011) 12850–12863.

[46] F. Larachi, J. Pierre, A. Adnot, A. Bernis, Ce 3d XPS study of composite $Ce_xMn_{1-x}O_{2-y}$ wet oxidation catalysts, Appl. Surf. Sci. 195 (2002) 236–250.

[47] Y. Li, Q. Sun, M. Kong, W. Shi, J. Huang, J. Tang, X. Zhao, Coupling oxygen ion conduction to photocatalysis in mesoporous nanorod-like ceria significantly improves photocatalytic efficiency, J. Phys. Chem. C 115 (2011) 14050–14057.

[48] H. Li, G. Qi, Tana, X. Zhang, X. Huang, W. Li, W. Shen, Low-temperature oxidation of ethanol over a $Mn_{0.6}Ce_{0.4}O_2$ mixed oxide, Appl. Catal. B: Environ. 103 (2011) 54–61.

[49] C. Zhang, C. Wang, W. Zhan, Y. Guo, Y. Guo, G. Lu, A. Baylet, A. Giroir-Fendler, Catalytic oxidation of vinyl chloride emission over $LaMnO_3$ and $LaB_{0.2}Mn_{0.8}O_3$ (B = Co, Ni Fe) catalysts, Appl. Catal. B: Environ. 129 (2013) 509–516.

[50] H. Li, G. Lu, Q. Dai, Y. Wang, Y. Guo, Y. Guo, Efficient low-temperature catalytic combustion of trichloroethylene over flower-like mesoporous Mn-doped CeO_2 microspheres, Appl. Catal. B: Environ. 102 (2011) 475–483.

[51] B.M. Reddy, L. Katta, G. Thrimurthulu, Novel nanocrystalline $Ce_{1-x}La_xO_{2-}(x = 0.2)$ solid solutions: structural characteristics and catalytic performance, Chem. Mater. 22 (2010) 467–475.

[52] J. Xu, P. Li, X. Song, C. He, J. Yu, Y. Han, Operando raman spectroscopy for determining the active phase in one-Dimensional $Mn_{1-x}Ce_xO_{2 \pm y}$ nanorod catalysts during methane combustion, J. Phys. Chem. Lett. 1 (2010) 1648–1654.

[53] C. Julien, M. Massot, S. Rangan, M. Lemal, D. Guyomard, Study of structural defects in γ-MnO_2 by Raman spectroscopy, J. Raman Spectrosc. 33 (2002) 223–228.

[54] T. Taniguchi, T. Watanabe, N. Sugiyama, A.K. Subramani, H. Wagata, N. Matsushita, Identifying defects in ceria-Based nanocrystals by UV resonance raman spectroscopy, J. Phys. Chem. C 113 (2009) 19789–19793.

[55] M. Luo, Z. Yan, L. Jin, M. He, Raman spectroscopic study on the structure in the surface and the bulk shell of $Ce_xPr_{1-x}O_{2-8}$ mixed oxides, J. Phys. Chem. B 110 (2006) 13068–13071.

[56] Z. Wu, M. Li, J. Howe, H.M. Meyer, S.H. Overbury, Probing defect sites on CeO_2 nanorystals with well-Defined surface plane by raman spectroscopy and O_2 adsorption, Langmuir 26 (2010) 16595–16606.

[57] Y. Lee, G. He, A.J. Akey, R. Si, M. Flytzani-Stephanopoulos, I.P. Herman, Raman analysis of mode softening in nanoparticle CeO_{2-8} and Au-CeO_{2-8} during CO oxidation, J. Am. Chem. Soc. 133 (2011) 12952–12955.

[58] Z. Pu, J. Lu .M. Luo, Y. Xie, Study of oxygen vacancies in $Ce_{0.9}Pr_{0.1}O_{2-(}$ solid solution by in situ X-ray diffraction and in situ raman spectroscopy, J. Phys. Chem. C 111 (2007) 18695–18702.

[59] J.A. Sullivan, P. Dulgheru, I. Atribak, A. Bueno-Lopez, A. Garcia-Garcia, Attempts at an in situ Raman study of ceria/zirconia catalysts in PM combustion, Appl. Catal. B: Environ. 108–109 (2011) 134–139.